


Using nonclassical states to explore the superradiant phase transition in the quantum Rabi model

Junpeng Liu ^{1,2} Miaomiao Zhao,^{1,2} Yun-Tong Yang,^{1,2} and Hong-Gang Luo^{1,2,3,*}¹*School of Physical Science and Technology, Lanzhou University, Lanzhou 730000, China*²*Lanzhou Center for Theoretical Physics and Key Laboratory of Theoretical Physics of Gansu Province, Lanzhou University, Lanzhou 730000, China*³*Beijing Computational Science Research Center, Beijing 100084, China*

(Received 6 December 2022; revised 16 January 2024; accepted 24 January 2024; published 27 February 2024)

The ground state of the quantum Rabi model (QRM) exhibits rich nonclassical states including the squeezed state, cat state, and entangled state in different parameter regimes. In this paper, we first use the polaron picture with high precision and fidelity to figure out the process of the superradiant phase transition (SPT) in view of the nonclassical states. The squeezing effect is considered to be a result of the higher-order excitations and important in order to understand the fundamental quantum physics of the SPT in the QRM. According to the polaron wave functions, the squeezed state extends across the entire range of parameters. Based on the squeezing and superradiance, a classification of the coupling strength for the nonclassical states containing the ground state is presented; the system sequentially goes through the vacuum states, the squeezed vacuum states, the squeezed cat states, and the cat states as the coupling strength increases. The process of the SPT is also demonstrated by the photon number distribution in Fock space, and then the novel behavior of parity chains for the SPT is revealed. Additionally, the nonclassical states can be intuitively characterized by the Wigner functions with analytical expressions in the polaron picture, and the Wigner negativity is evaluated to measure the nonclassicality. We find that a small but nonzero weighted antipolaron is necessary to form novel semicat states. Our paper provides guidance for preparing nonclassical states in experiments based on the light-matter interaction.

DOI: [10.1103/PhysRevA.109.023721](https://doi.org/10.1103/PhysRevA.109.023721)

I. INTRODUCTION

The quantum Rabi model (QRM) [1] plays an important role in understanding the fundamental physics in the field of light-matter interaction, which describes the coupling of a harmonic oscillator with frequency $\hbar\omega$ for a single-mode light field in the cavity and a two-level atom with frequency Δ , where the coupling strength is g . Despite its simple form, the analytical solutions with closed-form expressions for the general energy eigenvalues of the QRM are still difficult to obtain [2,3], which hinders physical exploration of the QRM. The well-known Jaynes-Cummings model (JCM) [4] is obtained by rotating-wave approximation (RWA), but is only justified for near-resonant ($\hbar\omega \approx \Delta$) and weakly coupled ($g \ll \hbar\omega$) parametric regions. For the cavity quantum electrodynamics, the coupling strength is usually limited, and in this case the JCM is successful in understanding a range of experimental phenomena, such as quantum Rabi oscillation [5] and vacuum Rabi mode splitting [6]. Thanks to the flexible tunability of various artificial systems, quantum simulation can lead to further increase in coupling strength, and then the RWA is invalid when the coupling strength becomes comparable to or even greater than the transition frequencies in the system, corresponding to ultrastrong coupling ($g \gtrsim 0.1\hbar\omega$) [7–9] and deep-strong coupling ($g \gtrsim \hbar\omega$) [10–12], respectively. One notes that this classification is just a historical

convention, and there is no deeper physical meaning [13]. While the classification based on the near-resonant condition is widely applicable [14], it is not suitable for other parametric regions, such as superradiant phase transition (SPT) with the condition of the ratio of the frequencies $\Delta/(\hbar\omega) \rightarrow \infty$ [15,16].

Recently, the SPT has been experimentally simulated by a single trapped ion [17,18] and a nuclear magnetic resonance [19], respectively, with large ratios $\Delta/(\hbar\omega) = 100$ and 50. Besides the SPT occurring in the ground state of the QRM as the coupling strength increases across the critical coupling strength, there are several kinds of nonclassical states existing in corresponding parametric regions, including the squeezed state, cat state, and entangled state [20–22]. The nonclassical states have wide applications in modern quantum technologies, such as the cat states for quantum computing [23–25], the entangled states for quantum information processing [26–28], and the squeezed states for quantum metrology [29–32]. In this paper, we explore a classification of parametric regions suitable for the SPT in the ground state of the QRM with well-defined physical meanings in view of the properties of the nonclassical states and figure out corresponding process of the SPT by characterizing the photon populations in Fock space [33], which can provide a guidance for preparing the nonclassical states in experiments based on the light-matter interaction. In particular, we reveal novel behavior of parity chains for the SPT in the QRM, which is important for understanding the fundamental quantum physics.

*luohg@lzu.edu.cn

The paper is organized as follows. In Sec. II, we numerically calculate the exact ground-state wave function and Wigner function for the QRM, and different nonclassical states in the process of the SPT are observed. In Sec. III, the improved polaron picture with high precision and fidelity is given, and the properties of the nonclassical states within all parameter ranges are demonstrated in detail. We discuss the nonclassical states corresponding to different coupling strength intervals based on the squeezing and superradiance, and obtain a classification to understand the process of the SPT by characterizing the photon populations in Fock space, then the novel behavior of the parity chains for the SPT is revealed in the QRM. In Sec. IV, the analytical expressions of the Wigner function are derived to characterize the nonclassical states and the Wigner negativity is calculated to measure the nonclassicality for the ground state. We find that a small but nonzero weighted antipolaron is necessary for leading to the semicat states. A brief conclusion is finally given in Sec. V.

II. THE NUMERICALLY EXACT CALCULATIONS FOR THE SPT OF THE QRM

The properties of the wave function have received little attention in the SPT [22], but the properties of the ground state change significantly with increasing coupling strength during SPT of the QRM, which is manifested as transitions between the nonclassical states. By characterizing the nonclassical states contained in the ground state, we can figure out the process of the SPT. In this section, we numerically calculate the exact ground-state wave function and the corresponding Wigner function to extract the physical picture in the process of the SPT of the QRM. The numerically exact results are usually used as a benchmarks to ensure and verify the accuracy and rationality of the analytical methods.

The QRM describes a quantized harmonic oscillator for a single-mode light field in the cavity coupled to a quantum two-level system for the atom; the Hamiltonian reads

$$\hat{H} = \hbar\omega\hat{a}^\dagger\hat{a} + \frac{\Delta}{2}\hat{\sigma}_z + g\hat{\sigma}_x(\hat{a}^\dagger + \hat{a}), \quad (1)$$

where \hat{a}^\dagger and \hat{a} are respectively the creation and annihilation operators for the harmonic oscillator with frequency $\hbar\omega$, the two-level system is described by Pauli matrices $\hat{\sigma}_{x,z}$ with the frequency Δ , and g is coupling strength between the two-level system and the quantum oscillator. For the SPT, the semiclassical critical strength $g_{c0} = \sqrt{\hbar\omega\Delta}/2$ divides the normal phase and the superradiant phase [15,20,34]. As an improved coupling scale compared to g_{c0} , the critical point $g_c = \sqrt{(\hbar\omega)^2 + (\hbar\omega)^4 + g_{c0}^4}$ from the shift of the semiclassical critical strength at finite frequencies is associated with the maximum of squeezing in the polaron picture [35], which is more suitable for exploring nonclassical states and is applied to a wider range of the parameters. Note that g_c approaches g_{c0} when the ratio of the frequencies $\Delta/(\hbar\omega) \rightarrow \infty$.

The exact wave function of the ground state of the QRM takes the form

$$\Psi_{\text{exact}} = \sum_{n=0}^{N_{\text{tr}}} (C_n^+ |n, \uparrow\rangle_x + C_n^- |n, \downarrow\rangle_x), \quad (2)$$

where C_n^\pm are coefficients, the superscripts \pm are respectively related to spin up $|\uparrow\rangle_x$ and spin down $|\downarrow\rangle_x$ in the x direction, the subscript n is related to Fock state $|n\rangle$, and N_{tr} is the truncated boson number in the Fock space.

The position representation of the Fock state of the field $|n\rangle$ is the usual harmonic oscillator

$$\langle x|n\rangle = (2^n n! \sqrt{\pi/\omega})^{-1/2} \exp(-\omega x^2/2) H_n(\sqrt{\omega}x), \quad (3)$$

where $H_n(\sqrt{\omega}x)$ are Hermite polynomials of order n . The ground-state wave function in the position representation is

$$\Psi_{\text{exact}} = \psi_+ |\uparrow\rangle_x + \psi_- |\downarrow\rangle_x, \quad (4)$$

where $\psi_\pm = \psi(\pm x) = \sum_{n=0}^{N_{\text{tr}}} C_n^\pm \langle x|n\rangle$.

As an important means to characterize nonclassical states, the Wigner function is experimentally measurable in light-matter interaction systems [19,23]. To characterize the nonclassical states contained in the process of the SPT for the QRM, we calculate the Wigner function:

$$W(x, p) = \frac{1}{\pi} \int_{-\infty}^{\infty} dx' \Psi_{\text{exact}}(x-x') \Psi_{\text{exact}}(x+x') e^{2ix'p}. \quad (5)$$

Figures 1(a)–1(d) show the numerically exact results (QUTIP) [36] of Wigner functions for different coupling strengths with the ratio $\Delta/(\hbar\omega) = 100$; it can be seen that the ground state exhibits the properties of the (a) vacuum state (VS), (b) squeezed vacuum state (SVS), (c) squeezed cat state (SCS), and (d) cat state (CS) as the coupling strength increases. Therefore, a rough phase diagram for the SPT of the QRM in view of the nonclassical states is extracted via the numerical Wigner function.

III. THE POLARON PICTURE FOR THE SPT OF THE QRM

Although numerically exact calculations can extract a rough physical picture, more details still require the help of some approximation methods to understand the physical process of the SPT in the QRM. As a powerful and effective method to investigate the properties of the ground state, the variational method is widely used in the study of the QRM [21,22,35,37–40]. The polaron picture is a useful method for extracting the ground-state wave function of the QRM [35,41] and its extensions [42–44]. In this section, an improved polaron picture is used to investigate the properties of the nonclassical states contained in the ground state for the SPT regime of the QRM.

A. The wave function and energy of the ground state over the entire range of parameters

We rewrite the part of the Hamiltonian (1) about the quantum oscillator in the position and momentum (x, p) representation, and expand the part about the two-level system in the basis of the σ_x representation. In terms of the creation

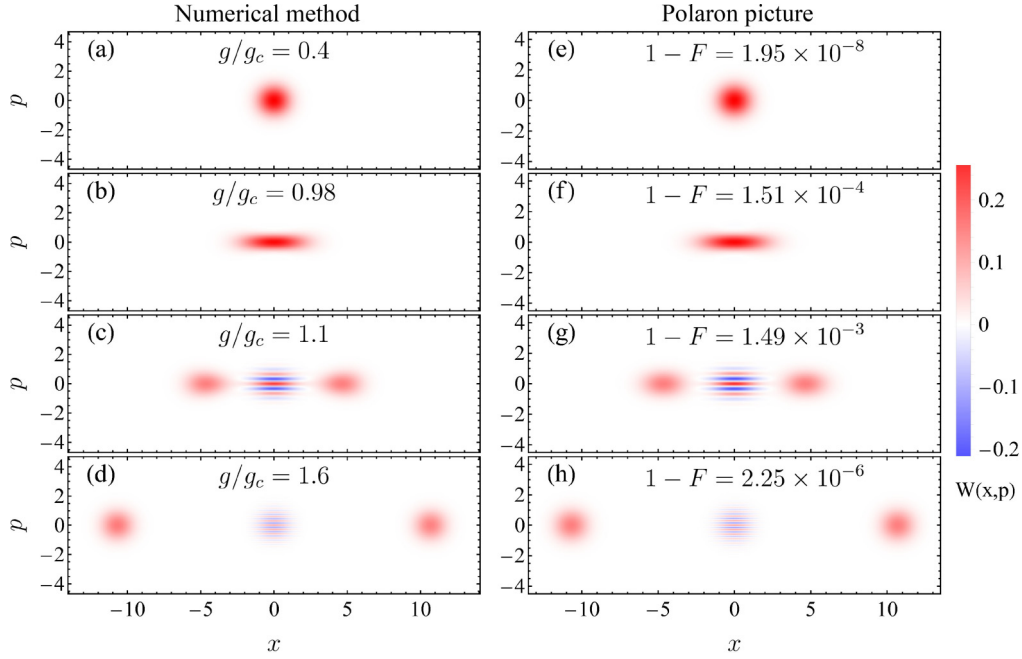


FIG. 1. The Wigner function $W(x, p)$ for the ground state by using the numerical method (a–d) and the polaron picture (e–h) for different coupling strengths. It can be seen that these characteristics are provided with nonclassical states: (a, e) vacuum state, (b, f) squeezed vacuum state, (c, g) squeezed cat state, and (d, h) cat state. The parameters are $\Delta/(\hbar\omega) = 100$ and (a, e) $g/g_c = 0.4$, (b, f) $g/g_c = 0.98$, (c, g) $g/g_c = 1.1$, and (d, h) $g/g_c = 1.6$.

and annihilation operators of the quantum harmonic oscillator with dimensionless formalism $\hat{a}^\dagger = (\hat{x} - i\hat{p})/\sqrt{2}$, $\hat{a} = (\hat{x} + i\hat{p})/\sqrt{2}$, where $\hat{x} = x$ and $\hat{p} = -i\frac{\partial}{\partial x}$ denote the position and momentum operators, respectively, the Hamiltonian (1) becomes

$$\hat{H} = \sum_{\sigma_x = \pm} \left(\hat{h}^{\sigma_x} |\sigma_x\rangle \langle \sigma_x| + \frac{\Delta}{2} |\sigma_x\rangle \langle \bar{\sigma}_x| \right) + \varepsilon_0, \quad (6)$$

where $\bar{\sigma}_x = -\sigma_x$, and $+$ ($-$) labels the state $|\uparrow\rangle_x$ ($|\downarrow\rangle_x$) of spin in the σ_x representation. $\hat{h}^\pm = \hbar\omega(\hat{p}^2 + \hat{v}_\pm)/2$, where $\hat{v}_\pm = [\hat{x} \pm \sqrt{2g/(\hbar\omega)}]^2$, and $\varepsilon_0 = -g^2/(\hbar\omega) + \hbar\omega/2$.

The ground-state wave function Ψ_x satisfies the Schrödinger equation $\hat{H}\Psi_x = E\Psi_x$, thus it should take the form

$$\Psi_x = \frac{1}{\sqrt{2}} (\psi_+ |\uparrow\rangle_x - \psi_- |\downarrow\rangle_x), \quad (7)$$

where $\psi_\pm = \psi(\pm x)$.

Originally, the method of the adiabatic approximation for the QRM [45] is based on the displaced oscillator picture, and the higher-order excitations are neglected under the condition $\Delta \ll \hbar\omega$. The squeezing effect such as the higher-order excitations is considered in various variational methods [21,22,35,37,41] to explore the ground state beyond the displaced oscillator picture, and the range of parameters applicable to these methods can be extended to the conditions of SPT for the QRM. In the polaron picture, the effect of higher-order excitations can be considered as an effective potential under the condition $\Delta \gg \hbar\omega$. The trial variational wave function for $\psi(x)$ takes the superposition of the deformed

polaron φ_α and antipolaron φ_β :

$$\begin{aligned} \psi(x) &= \alpha\varphi_\alpha(x) + \beta\varphi_\beta(x) \\ &= \alpha \left(\frac{\xi}{\pi} \right)^{\frac{1}{4}} \exp \left[-\frac{\xi(x - D_\alpha)^2}{2} \right] \\ &\quad + \beta \left(\frac{\xi}{\pi} \right)^{\frac{1}{4}} \exp \left[-\frac{\xi(x + D_\beta)^2}{2} \right], \end{aligned} \quad (8)$$

where $D_i = \zeta_i g'$ denotes displacements of the polarons, and $i = \alpha, \beta$ are respectively weights of the polaron and antipolaron with the same squeezed parameter ξ , which differs from two polarons with different squeezed parameters in Ref. [35]. Note that ψ_\pm in the ground-state wave function (7) are generalized cat states [23] with the squeezing when the polarons have nonzero displacements, which allow different weights for the coherent contributions, and satisfy that $\psi_+(x) = \psi_-(-x)$.

The wave function Eq. (7) satisfies the normalization condition, i.e.,

$$\langle \Psi_x | \Psi_x \rangle = \langle \psi_\pm | \psi_\pm \rangle = 1, \quad (9)$$

thus the probabilities of the two-level system in state $|\uparrow\rangle_x$ and $|\downarrow\rangle_x$ are independent of the parameters. The weight of the antipolaron β can be solved by the normalization condition Eq. (9), thus only four independent variational parameters $\{\alpha, \xi, \zeta_\alpha, \zeta_\beta\}$ are required by extracting from the energy minimization:

$$\frac{\partial E}{\partial \alpha} = \frac{\partial E}{\partial \xi} = \frac{\partial E}{\partial \zeta_\alpha} = \frac{\partial E}{\partial \zeta_\beta} = 0, \quad (10)$$

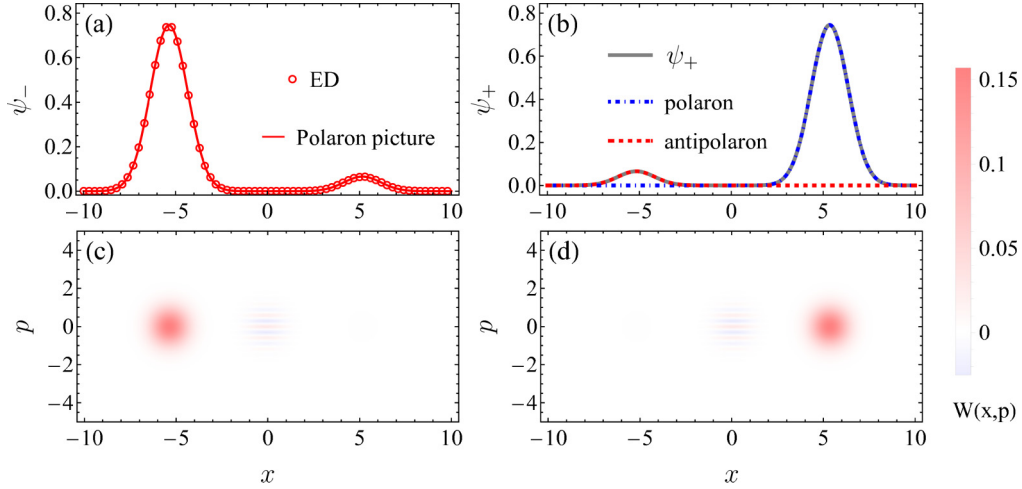


FIG. 2. The wave functions and corresponding Wigner functions in σ_x representation by using the polaron picture for the ground state of the QRM. (a) The wave function of the state ψ_- , which is in agreement with ED. (b) The wave function of the state ψ_+ , which consists of a polaron and an antipolaron. (c) Wigner function W_x^- of the state ψ_- . (d) Wigner function W_x^+ of the state ψ_+ . The parameters are $\Delta/(\hbar\omega) = 10$, $g/g_c = 2.0$, $\alpha = 0.996$, $\beta = 0.087$.

and the ground-state energy can be obtained as

$$\begin{aligned}
 E &= \langle \Psi | H | \Psi \rangle = \langle \psi_+ | h^+ | \psi_+ \rangle - \frac{\Delta}{2} \langle \psi_+ | \psi_- \rangle + \varepsilon_0 \\
 &= \frac{\hbar\omega}{2} [\alpha^2 (U_{-\alpha}^\alpha + V_{-\alpha}^\alpha) + \beta^2 (U_{-\beta}^\beta + V_{-\beta}^\beta) \\
 &\quad + 2\alpha\beta (U_{-\beta}^\alpha + V_{-\beta}^\alpha)] - \frac{\Delta}{2} (\alpha^2 + \beta^2 + 2\alpha\beta T_\beta^\alpha) + \varepsilon_0,
 \end{aligned} \tag{11}$$

where $F_{\pm j}^{\pm i} = F(\pm D_i, \pm D_j)$ is given by the functions

$$\begin{aligned}
 T(D_i, D_j) &= \exp\left[-\frac{(D_i + D_j)^2 \xi}{4}\right], \\
 U(D_i, D_j) &= T(D_i, D_j) \frac{2 + \xi(2g^2 - D_i + D_j)^2}{4\xi}, \\
 V(D_i, D_j) &= T(D_i, D_j) \frac{2\xi - \xi^2(D_i + D_j)^2}{4}.
 \end{aligned} \tag{12}$$

The energy error between the polaron picture and the exact result

$$\delta E = \left| \frac{E - E_{\text{exact}}}{E_{\text{exact}}} \right| \tag{13}$$

is obtained within all parameter ranges as shown in Fig. 3(a), which has an accuracy up to 10^{-4} . Figures 2(a) and 2(b) show the wave functions for the states ψ_{\mp} , respectively. The overlap with the variational wave function and the exact ones is defined as fidelity [21], i.e.,

$$F = |\langle \Psi_x | \Psi_{\text{exact}} \rangle|, \tag{14}$$

and we calculate the fidelity error $(1 - F)$ within all parameter ranges as shown in Fig. 3(b). It can be seen that the parameter range with the largest fidelity error does not exactly correspond to the range with the largest energy error, since the fidelity error is concentrated in the region where $|x| \rightarrow 0$ when $\Delta \gg \hbar\omega$, which is insensitive to energy minimization. The higher accuracy or fidelity can be obtained by using the

multipolaron expansion method with more variational parameters [41].

The multipolaron expansion [41] with more variational parameters can effectively improve the accuracy of the variational method; however, the smaller number of free parameters indicates that the state optimally captures the essential physics necessary to accurately describe the ground state [21]. Here we improve the polaron picture by reducing the variational parameters, and use it to analyze the properties of the nonclassical states in all parametric ranges, and then the squeezed region is distinguished [see Fig. 3(c)], which is extremely important because higher-order excitation represented by the squeezing effect is the key to cause the SPT of the QRM.

It is worth mentioning that the maximum squeezing at the critical point is crucial for the development of criticality-enhanced quantum metrology [46,47]. Figure 3(c) shows the squeezing parameter ξ as a function of the coupling strength g/g_c and the ratio $\Delta/(\hbar\omega)$ in all parameter ranges. When the ratio $\Delta/(\hbar\omega)$ is small ($\Delta/(\hbar\omega) \lesssim 1$), there is almost no squeezing in all regimes of the coupling strength; when the ratio $\Delta/(\hbar\omega)$ is large ($\Delta/(\hbar\omega) \gtrsim 10$), the squeezing occurs in the coupling strength interval of $0.5 \lesssim g/g_c \lesssim 1.5$, and reaches a maximum near the critical point g_c . Around the critical point, the larger the ratio $\Delta/(\hbar\omega)$, the greater the squeezing. To sum up, for the significant $\Delta/(\hbar\omega)$, with the increase of coupling strength, the squeezing increases continuously before the critical point, and reaches the maximum value near the critical point, then decreases after the critical point, and finally vanishes when the coupling strength becomes sufficiently strong.

B. The nonclassical states within the SPT and the classification for the ground state

The nonclassical states contained in the ground state of the QRM include the squeezed state, cat state, and entangled state [20–22], which have wide applications in modern

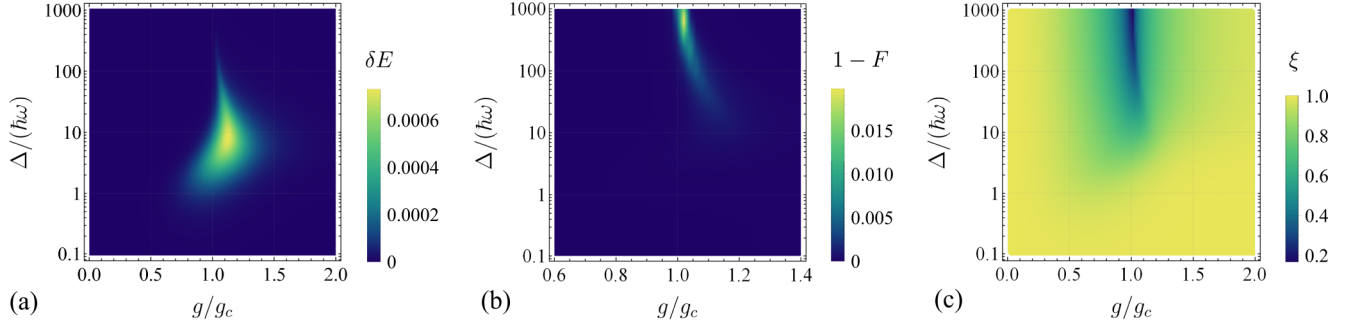


FIG. 3. The energy error, fidelity error, and squeezing parameter as functions of the coupling strength g/g_c and the ratio $\Delta/(\hbar\omega)$ for the ground state of the QRM in the polaron picture.

quantum technologies. In the following, we will analyze the property of the ground state from two aspects of cavity states and spin states, and calculate the related physical quantities to demonstrate the changes of the nonclassical states as functions of the coupling strength g/g_c and the ratio $\Delta/(\hbar\omega)$ in the SPT regime.

1. The x -type SPT caused by the cavity cat states

In σ_z representation, through Schmidt decomposition the form of ground-state wave function (7) of the QRM becomes

$$\Psi_z = \frac{1}{2}(\psi_O|\uparrow\rangle_z + \psi_E|\downarrow\rangle_z), \quad (15)$$

where

$$\begin{aligned} \psi_O &= \psi_+ - \psi_- = \alpha\Phi_\alpha^- - \beta\Phi_\beta^-, \\ \psi_E &= \psi_+ + \psi_- = \alpha\Phi_\alpha^+ + \beta\Phi_\beta^+, \end{aligned} \quad (16)$$

and $\Phi_i^\pm = \varphi_i(x) \pm \varphi_i(-x)$ respectively denote the even cat state (containing only even photon numbers) and odd cat state (containing only odd photon numbers) if $D_i > 0$. ψ_O and ψ_E are the linear superposition of the odd cat states and the even cat states [see Figs. 4(a) and 4(b)], respectively,

entangled with the spin-up state $|\uparrow\rangle_z$ and spin-down state $|\downarrow\rangle_z$ in Eq. (15), corresponding to the ground state belonging to the even-parity chain [48]:

$$|0, \downarrow\rangle_z \leftrightarrow |1, \uparrow\rangle_z \leftrightarrow |2, \downarrow\rangle_z \leftrightarrow |3, \uparrow\rangle_z \leftrightarrow \dots (p = +1). \quad (17)$$

The mean photon number of the ground state is always used as the order parameters of the SPT in the QRM [15,16], which undergoes abrupt changes from zero to finite numbers when the coupling strength goes through the critical point g_c in the limit $\Delta/(\hbar\omega) \rightarrow \infty$ (see Fig. 5), and the phenomena have been observed experimentally [17,19]. Note that the x -type SPT for the ground state of the QRM has been predicted by the qualitative analysis via the second-order perturbation theory in Ref. [16], and in the polaron picture the mean photon number of Eq. (15) can be given by

$$m = (\alpha^2 D_\alpha^2 + \beta^2 D_\beta^2)/2. \quad (18)$$

It is worth noting that the mean number of photons is only related to the sizes of the displacements and the weights of the polarons, and has nothing to do with the squeezing parameters. In Fig. 5, comparing the exact mean photon number (symbols) with m (solid lines), it can be seen that these are

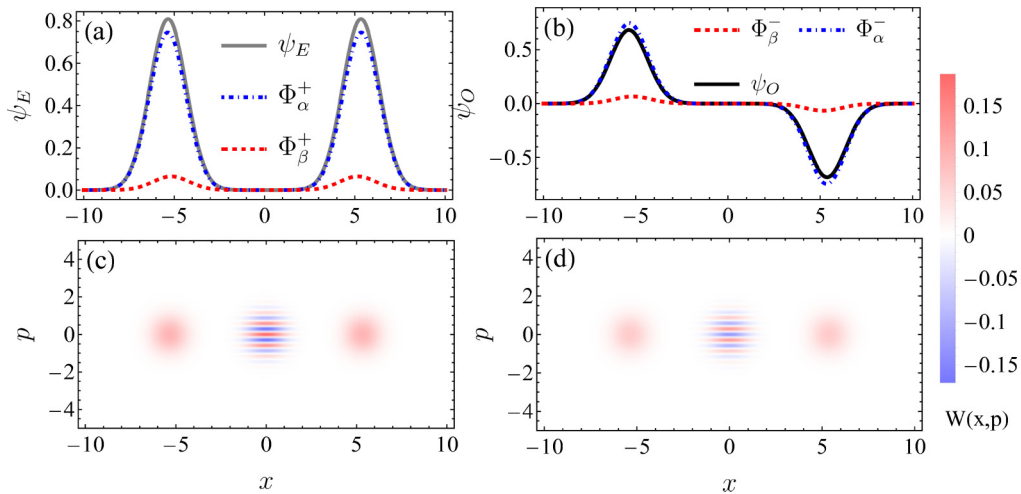


FIG. 4. The wave functions and corresponding Wigner functions in σ_z representation by using the polaron picture for the ground state of the QRM. (a) The wave functions of the even cat states in Eq. (15). (b) The wave functions of the odd cat states in Eq. (15). (c) The Wigner function W_z^E for the even cat state ψ_E entangled with $|\downarrow\rangle_z$. (d) The Wigner function W_z^O for the odd cat state ψ_O entangled with $|\uparrow\rangle_z$. The parameters are the same as in Fig. 2.

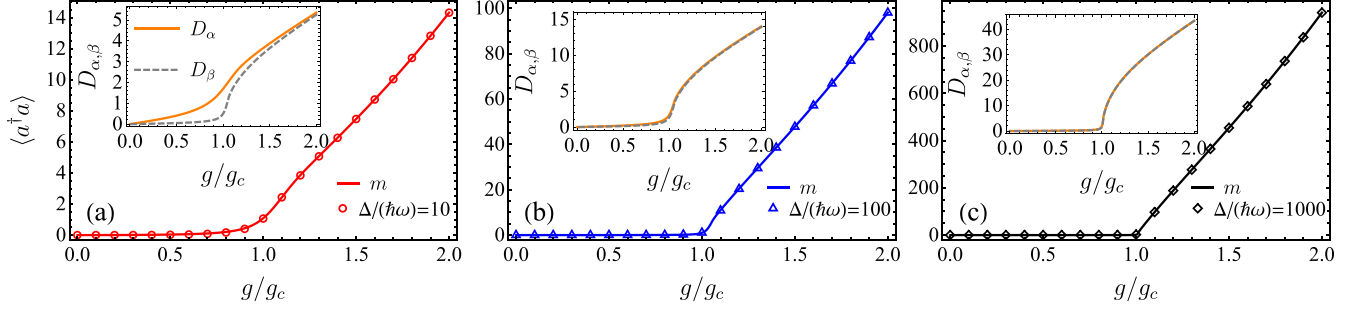


FIG. 5. (a–c) The exact mean photon number (symbols) vs m (solid lines) as functions of the coupling strength g/g_c of the ground state for $\Delta/(\hbar\omega) = 10, 100$, and 1000 , respectively. The symbols denote the numerically exact results. The insets are the displacements using the polaron picture as functions of the coupling strength g/g_c for the different ratio $\Delta/(\hbar\omega)$; the orange solid and gray dashed lines denote the displacements D_α and D_β , respectively.

very consistent for different $\Delta/(\hbar\omega)$. As shown in the insets of Fig. 5, when the system from the normal phase enters the superradiant phase, the displacements of two polarons undergo abrupt changes from zero to finite values for significant ratios [$\Delta/(\hbar\omega) \gtrsim 10$]. Moreover, for large ratios [$\Delta/(\hbar\omega) \gtrsim 100$], the displacement difference between the two polarons $\delta D = |D_\alpha - D_\beta| \rightarrow 0$, thus the behavior of superradiance in the QRM can be viewed as being caused by the same displacement of the cat states from zero to a finite value, i.e.,

$$\Psi_z = \frac{1}{2}[(\alpha - \beta)\Phi_\alpha^- | \uparrow \rangle_z + (\alpha + \beta)\Phi_\alpha^+ | \downarrow \rangle_z], \quad (19)$$

where only three independent variational parameters $\{\alpha, \xi, \zeta_\alpha\}$ are required in this case, and the mean photon number becomes

$$m = (\alpha^2 + \beta^2)D_\alpha^2/2. \quad (20)$$

Hence, for the SPT of the QRM, in the normal phase, the displacements of two polarons approaching zero lead to the vacuum states for the quantum oscillator [see Figs. 1(a) and 1(b)], and the nonzero displacements lead to the cat states in the superradiant phase [see Figs. 1(c) and 1(d)]. From Fig. 3(c), the ground state is squeezed around the critical point ($0.5 \lesssim g/g_c \lesssim 1.5$), thus there is the squeezed vacuum state before the critical point ($g/g_c \gtrsim 0.5$) and the squeezed cat states after the critical point ($g/g_c \lesssim 1.5$) as shown in Figs. 1(b) and 1(c), respectively. In the ranges of coupling strength $g/g_c \lesssim 0.5$ and $g/g_c \gtrsim 1.5$, the squeezing vanishes, and the cavity state consists of the vacuum states and the cat states, respectively.

2. The entangled state resulting from the emergence of the spin-up state

The population of the spin-up state $|\uparrow\rangle_z$ for the ground state is also used as the order parameters of the SPT in the QRM [15,17]. The probabilities of the states for the two-level system in σ_z representation are given by

$$P_\pm = \frac{1}{2}[\alpha^2(1 \mp T_\alpha^\alpha) + \beta^2(1 \mp T_\beta^\beta) \mp 2\alpha\beta T_\beta^\alpha (1/T_\gamma^\gamma \mp 1)], \quad (21)$$

where $\gamma = \sqrt{\alpha\beta}$, $P_+ = \langle \psi_O | \psi_O \rangle / 4$, and $P_- = \langle \psi_E | \psi_E \rangle / 4$ represent the probabilities of the spin-up state $|\uparrow\rangle_z$ and spin-down state $|\downarrow\rangle_z$, respectively. The probability P_+ as a function

of the coupling strength g/g_c for different $\Delta/(\hbar\omega)$ is indicated in Fig. 6(a), and $P_- = 1 - P_+$.

To measure entanglement between the harmonic oscillator and the two-level system in the ground state of the QRM, we calculate von Neumann entanglement entropy of the spin states by tracing out the cavity degree of freedom:

$$S = -(P_- \ln P_- + P_+ \ln P_+), \quad (22)$$

which is in good agreement with the numerical result as shown in Fig. 6(b). For the same coupling strength g , the smaller ratio $\Delta/(\hbar\omega)$ is, the larger the entanglement entropy is. When

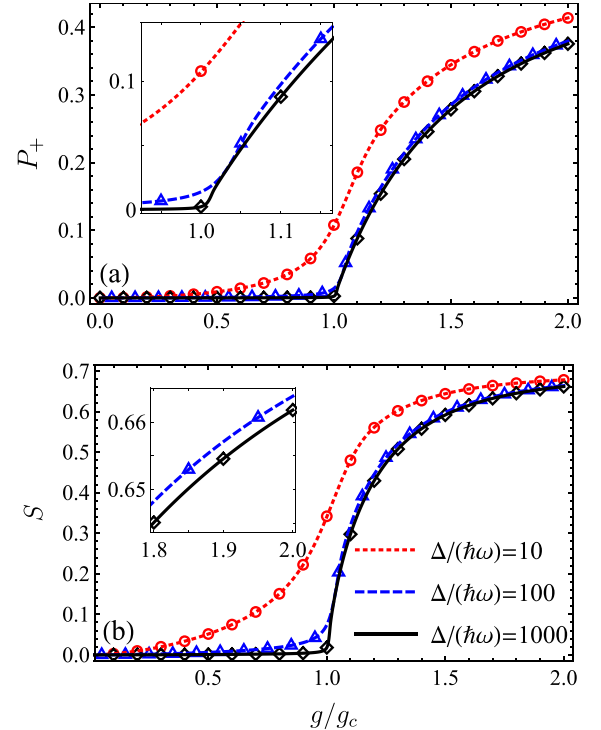


FIG. 6. The probability P_+ (a) and the von Neumann entanglement entropy (b) as functions of the coupling strength g/g_c for the ground state of the QRM with different ratio $\Delta/(\hbar\omega)$. The red dotted, blue dashed, and black solid lines are obtained by using the polaron picture for $\Delta/(\hbar\omega) = 10, 100$, and 1000 , respectively. The corresponding symbols denote the numerically exact results.

TABLE I. The nonclassical-state regions for the ground state of the QRM in the SPT regime.

$g/g_c \lesssim 0.5$	$0.5 \lesssim g/g_c \lesssim 1$	$1 \lesssim g/g_c \lesssim 1.5$	$g/g_c \gtrsim 1.5$
Normal phase		Superradiant phase	
Separable state		Entangled state	
Squeezed region			
VS	SVS	SCS	CS

the ratio $\Delta/(\hbar\omega) \rightarrow \infty$, the SPT occurs with increasing coupling strength, in the normal phase ($g < g_c$) $P_+ \rightarrow 0$, and the ground-state wave function $\Psi_z = \psi_E |\downarrow\rangle_z$ is a separable state, where the quantum oscillator is in the vacuum state and the two-level system is in the spin-down state $|\downarrow\rangle_z$; in the superradiant phase ($g > g_c$), the spin-up state $|\uparrow\rangle_z$ emerges [see Fig. 6(a)], and the ground state becomes entangled state (15), where the odd cat states ψ_O and the even cat states ψ_E are entangled with the spin-up state $|\uparrow\rangle_z$ and spin-down state $|\downarrow\rangle_z$, respectively.

From Fig. 6(b), it can be seen that the entanglement entropy increases more sharply from zero to a finite value near the critical point g_c for larger ratio $\Delta/(\hbar\omega)$, which can be used as the order parameter of the superradiant phase transition [16,34,49].

3. The classification for the ground state of the QRM

By analyzing the variational parameters of the ground-state wave function and calculating the related physical quantities for the SPT of the QRM, it can be seen that the boundaries between different nonclassical states based on the squeezing and superradiance are obvious when the ratio of the frequencies is relatively large [$\Delta/(\hbar\omega) \gtrsim 10$], thus the nonclassical-state regions for the ground state of the QRM in the SPT regime are distinguished as shown in Table I.

The squeezed region is in the coupling strength interval of $0.5 \lesssim g/g_c \lesssim 1.5$, and the critical point g_c divides the normal phase and superradiant phase. In the region of the normal phase, the ground state is the separable state, where the vacuum states of the quantum oscillator begin to be squeezed when $g/g_c \gtrsim 0.5$ and become squeezed vacuum states; while the two-level system is in the spin-down state, the squeezing increases with the coupling strength and reaches a maximum near g_c . In the region of the superradiant phase, the ground state becomes the entangled state; the squeezing starts to decrease and the displacements change from zero to finite values, correspondingly; the rapidly growing (in size) cat states with squeezing emerge, which consist of a large amount of the even cat states entangled with spin-down state and a small amount of the odd cat states entangled with the spin-up state. To further increase the coupling strength such that $g/g_c \gtrsim 1.5$, the squeezing vanishes, and the cavity state consists of the cat states. Hence, the ground state of the QRM in the SPT regime is divided into four regions in the coupling strength based on the properties of nonclassical states: VS, SVS, SCS, and CS.

C. The physical picture and the novel parity chains in the processes of the SPT for the QRM

To explore the physical picture of the SPT for the QRM, we calculate the photon number distribution in Fock space for the ground state as shown in Fig. 7. It can be seen that the number of photons is all in $|0\rangle$ for the vacuum states; the photon probability distribution for the squeezed vacuum states is only existing for the even photon numbers and vanishing for all odd photon numbers [50], which can be fitted by the Poissonian-like statistics; and the photon population in odd photon numbers arises for the squeezed odd cat states and odd cat states, together with the photon population in even photon numbers for the even counterparts, corresponding to the statistics of the Gaussian unitary ensemble (GUE) [33]. Notably, as coupling strength increases, the photon number distribution in Fock space changes from $|0\rangle$ to the distribution of the Fock states with only the even photon numbers, the squeezing builds up before the critical point and reaches a maximum near the critical point, while the mean number of photons of the ground state is zero; when the squeezing decreases after the critical point, the displacements of the two polarons occur and the mean number of photons increases dramatically. It is the accumulation of the squeezing that causes the photon number to have a nonzero population in the larger Fock states, therefore the distribution of the photon number is more likely to shift and thus form the displacements when the squeezing is released. In contrast to the case of the smaller ratio ($\Delta/(\hbar\omega) \lesssim 1$), there is no squeezing process with the coupling strength increasing, so the mean number of photons in the ground state increases smoothly.

Combined with the state of the two-level system in the light-matter interaction, we can figure out processes of the SPT with increasing coupling strength as transfer of the photon number population from $|0, \downarrow\rangle_z$ to the distribution of only the even photon numbers with Poissonian-like statistics leading to the accumulation of squeezing before the critical point g_c [see Figs. 8(a) and 8(b)]. The ground state changes from VS to SVS, the latter corresponding to the two-photon parity chain, i.e., $|0, \downarrow\rangle_z \leftrightarrow |2, \downarrow\rangle_z \leftrightarrow |4, \downarrow\rangle_z \leftrightarrow \dots$, indicated by the pink arrows in Fig. 8(b), and the squeezing reaches the maximum near the critical point. Then emergence of the spin-up state and GUE-like photon population within the odd photon numbers leading to the release of the squeezing after the critical point is accompanied by a sharp increase in the displacements after the critical point, i.e., $\dots \leftrightarrow |2n, \downarrow\rangle_z \leftrightarrow |2n+1, \uparrow\rangle_z \leftrightarrow |2n+2, \downarrow\rangle_z \leftrightarrow |2n+3, \uparrow\rangle_z \leftrightarrow \dots$, indicated by a chain of black arrows in Fig. 8(c); in addition, there is a two-photon chain on each of the two branches due to the squeezing effect, i.e., $\dots \leftrightarrow |2n, \downarrow\rangle_z \leftrightarrow |2n+2, \downarrow\rangle_z \leftrightarrow \dots$ and $\dots \leftrightarrow |2n+1, \uparrow\rangle_z \leftrightarrow |2n+3, \uparrow\rangle_z \leftrightarrow \dots$, respectively, indicated by a chain of pink and purple arrows; the three parity chains jointly form the ground-state wave function in Eq. (15), which consists of the SCS entangled with the spin states. When the squeezing effect disappears in the CS region, only the parity chain indicated by the black arrows remains. Note that these parity chains related to the squeezing effect do not affect the displacements of the polarons and the mean number of photons of the ground state due to the x -type SPT in the QRM.

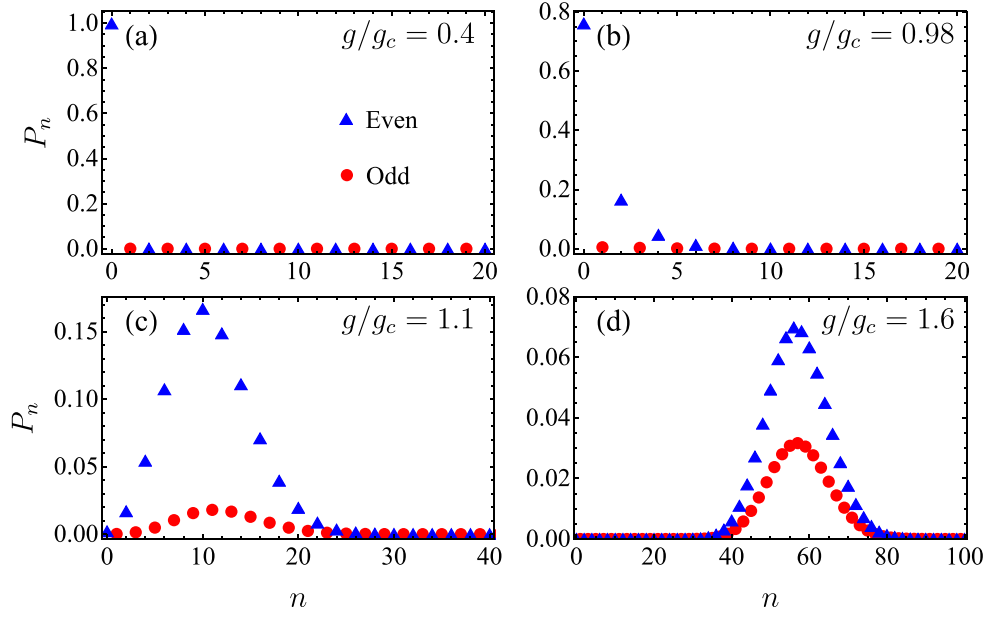


FIG. 7. The photon number distribution in Fock space for (a) the vacuum states, (b) the squeezed vacuum states, (c) the squeezed cat states, and (d) the cat states contained in the ground state. The red points and blue triangles denote the photon distribution in Fock basis with odd and even photon numbers, respectively. The parameters are the same as in Fig. 1.

For clarity, the parity chains of nonclassical-state regions for the SPT in the ground state of the QRM are shown in Table II. Interestingly, although the parity chains of the SPT corresponding to different coupling strengths are novel, these are included in the parity Eq. (17) to which the QRM ground state belongs, which confirms that this analysis based on the polaron picture is reasonable. Therefore, the physical picture of squeezing accumulation before the critical cou-

pling strength to squeezing release after the critical coupling strength is given for the SPT of the QRM.

From this perspective, we obtain that the squeezing effect is the key to the SPT for the QRM based on the improved polaron picture, which is considered to be the higher-order excitations. Unlike this case, the SPT in the Dicke model was found to be the collective behavior in the thermodynamic limit, where the polaron picture is no longer directly

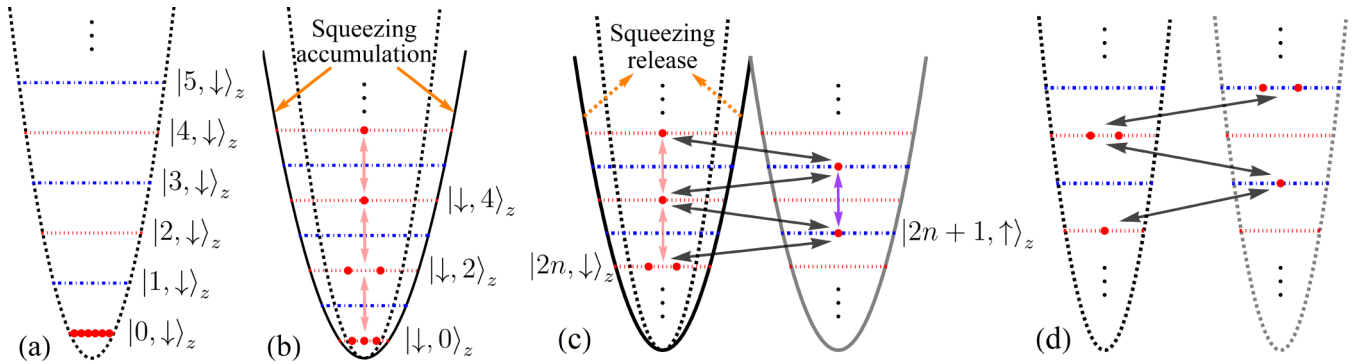


FIG. 8. Schematic diagram of the ground-state photon number distribution in Fock space for the SPT in the QRM. (a) VS: The vacuum states with only photon population for $|0\rangle$ in the branch of the spin-down state $|\downarrow\rangle_z$, i.e., $|0, \downarrow\rangle_z$. (b) SVS: The squeezing accumulation leading to the squeezed vacuum states with Poissonian-like photon distribution for the even photon numbers in the branch of $|\downarrow\rangle_z$, i.e., $|0, \downarrow\rangle_z \leftrightarrow |2, \downarrow\rangle_z \leftrightarrow |4, \downarrow\rangle_z \leftrightarrow \dots$, indicated by a chain of pink arrows, which is a two-photon chain. (c) SCS: The squeezing release leading to the emergence of the squeezed odd cat states with GUE-like photon distribution for the odd photon numbers in the branch of the spin-up state of $|\uparrow\rangle_z$, while the GUE-like photon distribution for even photon numbers forms the squeezed even cat states in the branch of $|\downarrow\rangle_z$, i.e., $\dots \leftrightarrow |2n, \downarrow\rangle_z \leftrightarrow |2n+1, \uparrow\rangle_z \leftrightarrow |2n+2, \downarrow\rangle_z \leftrightarrow |2n+3, \uparrow\rangle_z \leftrightarrow \dots$, indicated by a chain of black arrows; in addition, there is a two-photon chain on each of the two branches due to the squeezing effect, i.e., $\dots \leftrightarrow |2n, \downarrow\rangle_z \leftrightarrow |2n+2, \downarrow\rangle_z \leftrightarrow \dots$ and $\dots \leftrightarrow |2n+1, \uparrow\rangle_z \leftrightarrow |2n+3, \uparrow\rangle_z \leftrightarrow \dots$, indicated by a chain of pink and purple arrows, respectively. (d) CS: When the squeezing effect disappears, only the parity chain indicated by the black arrows remains. The black and gray dashed parabolic wells denote the potential of the harmonic oscillator without squeezing, the black and gray solid parabolic wells denote the potentials of the harmonic oscillator with squeezing, and black and gray correspond to the branches of the spin-down and spin-up states, respectively.

TABLE II. The parity chains of nonclassical-state regions for the SPT of the QRM.

VS	$ 0, \downarrow\rangle_z$
SVS	$ 0, \downarrow\rangle_z \leftrightarrow 2, \downarrow\rangle_z \leftrightarrow 4, \downarrow\rangle_z \leftrightarrow \dots$
SCS	$\dots \leftrightarrow 2n, \downarrow\rangle_z \leftrightarrow 2n+1, \uparrow\rangle_z \leftrightarrow 2n+2, \downarrow\rangle_z \leftrightarrow 2n+3, \uparrow\rangle_z \leftrightarrow \dots$ $\dots \leftrightarrow 2n, \downarrow\rangle_z \leftrightarrow 2n+2, \downarrow\rangle_z \leftrightarrow \dots$ $\dots \leftrightarrow 2n+1, \uparrow\rangle_z \leftrightarrow 2n+3, \uparrow\rangle_z \leftrightarrow \dots$
CS	$\dots \leftrightarrow 2n, \downarrow\rangle_z \leftrightarrow 2n+1, \uparrow\rangle_z \leftrightarrow 2n+2, \downarrow\rangle_z \leftrightarrow 2n+3, \uparrow\rangle_z \leftrightarrow \dots$

applicable; how to extend the present paper to the Dicke model is an interesting issue deserving further study in the future. The process of SPT in the QRM is also different from that of the JCM; the ground state for the normal phase of the latter is $|0, \downarrow\rangle_z$ before the critical point, and for the superradiant phase after the critical point is determined by the lower-energy states of adjacent JC doublets [51]; there are no special distributions like the QRM in the whole process of the SPT.

IV. WIGNER FUNCTIONS FOR THE GROUND STATE IN THE POLARON PICTURE

Although the Wigner function derived from the numerical method can qualitatively obtain the general properties of the nonclassical states contained in the ground state, for the analysis of the formation of the nonclassical states in the interaction system of light and matter, the Wigner function with an analytical form is indispensable. In this section, the Wigner functions with analytical expressions for the ground state of the QRM are obtained using the polaron picture.

A. The Wigner functions with analytical expressions

The expressions of the Wigner function for the wave functions ψ_{\pm} in σ_x representation can be obtained as

$$W_x^+ = W_\alpha^R + W_I^+ + W_\beta^L, \quad W_x^- = W_\alpha^L + W_I^- + W_\beta^R, \quad (23)$$

where

$$\begin{aligned}
 W_\alpha^R &= \frac{1}{2\pi} \alpha^2 N_{-\alpha}^{-\alpha}, & W_\beta^L &= \frac{1}{2\pi} \beta^2 N_\beta^\beta, \\
 W_\alpha^L &= \frac{1}{2\pi} \alpha^2 N_\alpha^\alpha, & W_\beta^R &= \frac{1}{2\pi} \beta^2 N_{-\beta}^{-\beta}, \\
 W_I^+ &= \frac{1}{\pi} \alpha \beta N_{-\beta}^\alpha M_\beta^\alpha, & W_I^- &= \frac{1}{\pi} \alpha \beta N_\beta^{-\alpha} M_{-\beta}^{-\alpha},
 \end{aligned} \quad (24)$$

and $F_{\pm j}^{\pm i} = F(\pm D_i, \pm D_j)$ is given by the functions

$$\begin{aligned}
 N(D_i, D_j) &= \exp\left[-\frac{(2p)^2 + (2x + D_i + D_j)^2 \xi^2}{4\xi}\right], \\
 M(D_i, D_j) &= \cos[(D_i + D_j)p].
 \end{aligned} \quad (25)$$

Note that $N(D_i, D_j)$ determine areas of the Wigner functions, and W_α^R (W_α^L) and W_β^R (W_β^L) are produced by the polaron φ_α and the antipolaron φ_β , respectively, and are on the right (left) side of the Wigner function, often referred to as ‘‘alive’’ (‘‘dead’’) states. W_I^\pm are the interference terms, where $M(D_i, D_j)$ determines oscillations of the Wigner functions. Intensities of the Wigner functions depend on the weights α and β . Figures 2(a) and 2(b) and Figs. 2(c) and 2(d) show

the wave functions and corresponding Wigner functions for the states ψ_{\mp} , respectively. From Eq. (25), the expression of the area term of Wigner functions depends on the squeezing parameters ξ ; the term containing coordinates grows more slowly than the term containing momentum if $\xi < 1$, thus causing the squeezing in the p direction [see Figs. 1(b) and 1(c)]; and the smaller ξ , the larger the squeezing. It turns out that the Wigner functions satisfy $W_x^\pm(x, p) = W_x^\mp(-x, p)$, since the wave functions satisfy $\psi_+(x) = \psi_-(-x)$. Therefore, the total Wigner function of the ground state in the polaron picture $W_T = W_x^+ + W_x^-$; the corresponding results are shown in Figs. 1(e)–1(h), which agree well with the numerical ones due to the high fidelities of the wave functions.

In σ_z representation, the Wigner functions for the cat states ψ_O and ψ_E can be obtained by

$$W_z^O = \frac{1}{2}W_T - W_D, \quad W_z^E = \frac{1}{2}W_T + W_D, \quad (26)$$

where

$$\begin{aligned}
 W_D &= \frac{1}{2\pi} [\alpha^2 N_0^0 M_\alpha^\alpha + \beta^2 N_0^0 M_\beta^\beta \\
 &\quad + \alpha \beta (N_{-\beta}^{-\alpha} M_\beta^{-\alpha} + N_\beta^\alpha M_{-\beta}^\alpha)].
 \end{aligned} \quad (27)$$

Figures 4(a) and 4(b) and Figs. 4(c) and 4(d) show the wave functions and corresponding Wigner functions for the two kinds of cat states, respectively. Moreover, the weight of the odd cat states is always less than that of the even cat states in superradiant phase due to the nonzero β [see Fig. 10(b)]; according to Eq. (15), the total Wigner function of the ground

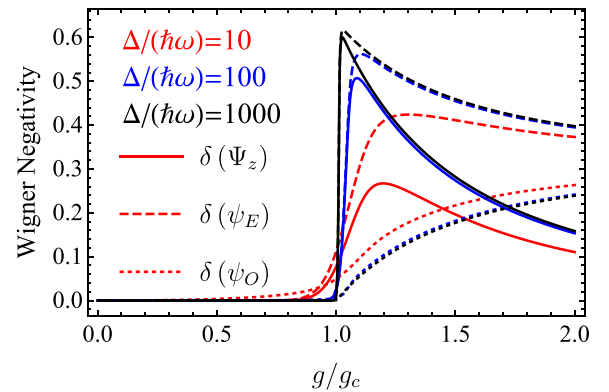


FIG. 9. The Wigner negativity by numerical integration of Eq. (28) as a function of the coupling strength g/g_c for different ratio $\Delta/(\hbar\omega)$. The solid, dashed, and dotted lines denote Wigner negativity for the Wigner functions of Ψ_z , Ψ_E , and Ψ_O , respectively; the red, blue, and black colors correspond to results of the ratio $\Delta/(\hbar\omega) = 10, 100, \text{ and } 1000$.

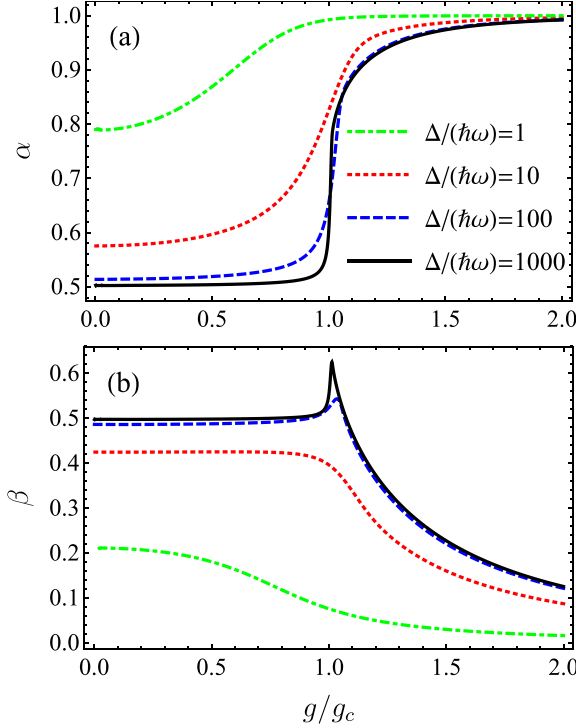


FIG. 10. The weights of the polaron (a) and the antipolaron (b) as functions of the coupling strength g/g_c for different $\Delta/(\hbar\omega)$. The green dot-dashed, red dotted, blue dashed, and black solid lines denote the weights for the ratio $\Delta/(\hbar\omega) = 1, 10, 100,$ and 1000 , respectively.

state is dominated by the even cat states and indicates the characteristic of the even cat states as shown in Fig. 1.

B. Wigner negativity for the ground state

The Wigner negativity is evaluated to measure nonclassicality for the cavity states [52], which is defined as

$$\delta(\psi) = \iint [|W_\psi(x, p)| - W_\psi(x, p)] dx dp. \quad (28)$$

In Fig. 9, we calculate the Wigner negativity for Wigner functions of the ground state by numerical integration; the solid, dashed, and dotted lines denote Wigner negativity for the Wigner functions W_T , W_z^E , and W_z^O corresponding to the wave functions of the ground state Ψ_z , the even state ψ_E , and the odd state ψ_O , respectively; the red, blue, and black colors correspond to results of the ratio $\Delta/(\hbar\omega) = 10, 100,$ and 1000 . The quantities of Wigner negativity are all equal to zero within the vacuum state and squeezed vacuum state when the coupling strength $g/g_c \lesssim 1$. For $g/g_c \gtrsim 1$ and larger ratio $\Delta/(\hbar\omega)$, $\delta(\Psi_z)$ and $\delta(\psi_E)$ increase more sharply around g_c ; both reach their larger maximum when the coupling strength is slightly greater than the critical point g_c and then start to decline, while $\delta(\psi_O)$ keeps growing but is smaller as the coupling strength increases. In addition, for the same $\Delta/(\hbar\omega)$, $\delta(\psi_E) > \delta(\Psi_z)$, and $\delta(\psi_E) > \delta(\psi_O)$ for $g/g_c > 1$, $\delta(\Psi_z)$ decreases faster than $\delta(\psi_E)$ due to $\delta(\psi_O)$ increasing with coupling strength. Further, $\delta(\psi_O) > \delta(\Psi_z)$ when the coupling strength reaches sufficiently strong ($g/g_c \gtrsim 1.5$).

Through the above analysis, we can obtain that the Wigner negativity for the ground state of the QRM is nonzero when the displacements $D_{\alpha,\beta} > 0$, and when the ratio $\Delta/(\hbar\omega)$ is larger the squeezing is larger, the values of $\delta(\Psi_z)$ and $\delta(\psi_E)$ are larger, and $\delta(\psi_O)$ is smaller. To sum up, the presence or absence of the displacements is decisive for the occurrence of nonclassicality of the cavity states, while the squeezing only affects its extreme value.

C. The necessary antipolaron with very small but nonzero weight leading to semicat states

In σ_x representation, ψ_\pm in the ground-state wave function (7) are generalized cat states [23] with the squeezing when the polarons have nonzero displacements, which allow different weights for the coherent contributions. As shown in Fig. 10(a) the weight of the polaron $\alpha \rightarrow 1$, and (b) the weight of the antipolaron β becomes small but nonzero when the coupling strength $g/g_c \gtrsim 1.5$. According to Eq. (23), the intensities of Wigner functions depend on the weights, and the intensities of interference term W_I^\pm depend on the product of the weights $\alpha\beta \rightarrow \beta$; meanwhile, $\beta^2 \rightarrow 0$, so that the Wigner functions belonging to the antipolaron in W_x^\pm vanish, i.e.,

$$\begin{aligned} W_x^+ &\rightarrow W_x^{\text{alive}} \equiv W_\alpha^R + W_I^+, \\ W_x^- &\rightarrow W_x^{\text{dead}} \equiv W_\alpha^L + W_I^-, \end{aligned} \quad (29)$$

where W_x^{alive} and W_x^{dead} denote alive and dead semicat states, which are the even cat states that exclude only the dead cat and alive cat parts as shown in Figs. 2(c) and 2(d), respectively. It can be seen that the interference fringes are clearly visible, which demonstrates that the composition of the small but nonzero antipolaron in the wave function (8) is necessary when the coupling strength is sufficiently strong ($g/g_c \gtrsim 1.5$).

In particular, as shown by the green dot-dashed line in Fig. 10(b), for the case of a smaller ratio $\Delta/(\hbar\omega)$, the weight $\beta \rightarrow 0$ under sufficiently strong coupling ($g/g_c \gtrsim 1.5$), leading to $W_I^\pm \rightarrow 0$; the interference fringes fade away, and the semicat states turn into corresponding coherent states; the ground-state wave function (7) becomes

$$\Psi_x = \frac{1}{\sqrt{2}} [\varphi_\alpha(x) |\uparrow\rangle_x - \varphi_\alpha(-x) |\downarrow\rangle_x], \quad (30)$$

where only one variational parameter $\{\zeta_\alpha\}$ is required.

The existence of generalized cat states in the QRM, including the odd cat states, even cat states, and exotic semicat states, as well as their squeezed counterparts, will provide more possibilities for quantum computing [23–25] and quantum information processing [26–28] based on the interaction between light and matter.

V. CONCLUSION

The squeezing effect is considered to be a result of the higher-order excitations, which is important in order to understand the fundamental quantum physics of the SPT in the QRM. In this paper, we study the nonclassical states contained in the ground state of the QRM using the polaron picture, where the variational wave function consists of a polaron and an antipolaron, which have the same squeezing parameter and are distinguished by different displacements and weights.

A squeezed region within all parameter ranges is distinguished, which corresponds to the region around the critical coupling strength ($0.5 \lesssim g/g_c \lesssim 1.5$) of the SPT in the model with a significant ratio [$\Delta/(\hbar\omega) \gtrsim 10$]. We find that the x -type SPT is dominated by the cat states with displacements of the same size increasing from zero to a finite value when the coupling strength goes through the critical point, while the ground state changes from a separated state to an entangled state. For the superradiant phase, a pair of novel semicat states caused by the necessary antipolaron with small but nonzero weight in sufficiently strong coupling ($g/g_c \gtrsim 1.5$) is revealed.

In the polaron picture, we give the interval of coupling strengths corresponding to the nonclassical states based on the squeezing and the superradiance; the cavity state sequentially goes through the VS, the SVS, the SCS, and the CS as the coupling strength increases. Moreover, by combining the analysis of the photon number distribution in Fock space for the ground state of the QRM, we clearly indicate the process of SPT, and we reveal novel parity chains for the SPT in the ground state

of the QRM. Therefore, a physical picture of the SPT resulting from higher-order excitations represented by the squeezing effect is established, which will aid our understanding of few-body quantum phase transition. Further, we derive analytical expressions of Wigner functions for the ground state of the QRM to characterize the nonclassical states, and calculate Wigner negativity and von Neumann entanglement entropy to measure nonclassicality and entanglement, respectively, which are important for modern quantum technologies.

ACKNOWLEDGMENTS

We thank Gang Liu, Fu-Zhou Chen, and Si-Yuan Bai for helpful discussions. We acknowledge funding from the National Key Research and Development Program of China (Grant No. 2022YFA1402704) and the National Natural Science Foundation of China (Grants No. 12247101 and No. 11834005).

-
- [1] I. I. Rabi, *Phys. Rev.* **51**, 652 (1937).
 - [2] P. Forn-Díaz, L. Lamata, E. Rico, J. Kono, and E. Solano, *Rev. Mod. Phys.* **91**, 025005 (2019).
 - [3] Z.-M. Li and M. T. Batchelor, *Phys. Rev. A* **104**, 033712 (2021).
 - [4] E. T. Jaynes and F. W. Cummings, *Proc. IEEE* **51**, 89 (1963).
 - [5] M. Brune, F. Schmidt-Kaler, A. Maali, J. Dreyer, E. Hagley, J. M. Raimond, and S. Haroche, *Phys. Rev. Lett.* **76**, 1800 (1996).
 - [6] R. J. Thompson, G. Rempe, and H. J. Kimble, *Phys. Rev. Lett.* **68**, 1132 (1992).
 - [7] A. A. Anappara, S. De Liberato, A. Tredicucci, C. Ciuti, G. Biasiol, L. Sorba, and F. Beltram, *Phys. Rev. B* **79**, 201303(R) (2009).
 - [8] T. Niemczyk, F. Deppe, H. Huebl, E. P. Menzel, F. Hocke, M. J. Schwarz, J. J. Garcia-Ripoll, D. Zueco, T. Hümmer, E. Solano, A. Marx, and R. Gross, *Nat. Phys.* **6**, 772 (2010).
 - [9] P. Forn-Díaz, J. J. García-Ripoll, B. Peropadre, J. L. Orgiazzi, M. A. Yurtalan, R. Belyansky, C. M. Wilson, and A. Lupascu, *Nat. Phys.* **13**, 39 (2017).
 - [10] S. De Liberato, *Phys. Rev. Lett.* **112**, 016401 (2014).
 - [11] N. K. Langford, R. Sagastizabal, M. Kounalakis, C. Dickel, A. Bruno, F. Luthi, D. J. Thoen, A. Endo, and L. DiCarlo, *Nat. Commun.* **8**, 1715 (2017).
 - [12] F. Yoshihara, T. Fuse, S. Ashhab, K. Kakuyanagi, S. Saito, and K. Semba, *Nat. Phys.* **13**, 44 (2017).
 - [13] A. Frisk Kockum, A. Miranowicz, S. De Liberato, S. Savasta, and F. Nori, *Nat. Rev. Phys.* **1**, 19 (2019).
 - [14] D. Z. Rossatto, C. J. Villas-Bôas, M. Sanz, and E. Solano, *Phys. Rev. A* **96**, 013849 (2017).
 - [15] M.-J. Hwang, R. Puebla, and M. B. Plenio, *Phys. Rev. Lett.* **115**, 180404 (2015).
 - [16] M. Liu, S. Chesi, Z.-J. Ying, X. Chen, H.-G. Luo, and H.-Q. Lin, *Phys. Rev. Lett.* **119**, 220601 (2017).
 - [17] M. L. Cai, Z. D. Liu, W. D. Zhao, Y. K. Wu, Q. X. Mei, Y. Jiang, L. He, X. Zhang, Z. C. Zhou, and L. M. Duan, *Nat. Commun.* **12**, 1126 (2021).
 - [18] M. L. Cai, Z. D. Liu, Y. Jiang, Y. K. Wu, Q. X. Mei, W. D. Zhao, L. He, X. Zhang, Z. C. Zhou, and L. M. Duan, *Chin. Phys. Lett.* **39**, 020502 (2022).
 - [19] X. Chen, Z. Wu, M. Jiang, X. Y. Lu, X. Peng, and J. Du, *Nat. Commun.* **12**, 6281 (2021).
 - [20] S. Ashhab and F. Nori, *Phys. Rev. A* **81**, 042311 (2010).
 - [21] C. Leroux, L. C. G. Govia, and A. A. Clerk, *Phys. Rev. A* **96**, 043834 (2017).
 - [22] X.-Y. Chen, Y.-Y. Zhang, L. Fu, and H. Zheng, *Phys. Rev. A* **101**, 033827 (2020).
 - [23] B. Hacker, S. Welte, S. Daiss, A. Shaikat, S. Ritter, L. Li, and G. Rempe, *Nat. Photon.* **13**, 110 (2019).
 - [24] M. Bergmann and P. van Loock, *Phys. Rev. A* **94**, 042332 (2016).
 - [25] A. Grimm, N. E. Frattini, S. Puri, S. O. Mundhada, S. Touzard, M. Mirrahimi, S. M. Girvin, S. Shankar, and M. H. Devoret, *Nature (London)* **584**, 205 (2020).
 - [26] L. Li, C.-L. Zou, V. V. Albert, S. Muralidharan, S. M. Girvin, and L. Jiang, *Phys. Rev. Lett.* **119**, 030502 (2017).
 - [27] V. V. Albert, C. Shu, S. Krastanov, C. Shen, R.-B. Liu, Z.-B. Yang, R. J. Schoelkopf, M. Mirrahimi, M. H. Devoret, and L. Jiang, *Phys. Rev. Lett.* **116**, 140502 (2016).
 - [28] F.-X. Sun, S.-S. Zheng, Y. Xiao, Q. Gong, Q. He, and K. Xia, *Phys. Rev. Lett.* **127**, 087203 (2021).
 - [29] J. Joo, W. J. Munro, and T. P. Spiller, *Phys. Rev. Lett.* **107**, 083601 (2011).
 - [30] J. Hastrup, K. Park, R. Filip, and U. L. Andersen, *Phys. Rev. Lett.* **126**, 153602 (2021).
 - [31] C. Sánchez Muñoz and D. Jaksch, *Phys. Rev. Lett.* **127**, 183603 (2021).
 - [32] M. Xin, W. S. Leong, Z. Chen, Y. Wang, and S.-Y. Lan, *Phys. Rev. Lett.* **127**, 183602 (2021).
 - [33] Y.-T. Yang and H.-G. Luo, *Chinese Phys. Lett.* **40**, 020502 (2023).
 - [34] S. Ashhab, *Phys. Rev. A* **87**, 013826 (2013).
 - [35] Z.-J. Ying, M. Liu, H.-G. Luo, H.-Q. Lin, and J. Q. You, *Phys. Rev. A* **92**, 053823 (2015).

- [36] J. Johansson, P. Nation, and F. Nori, *Comput. Phys. Commun.* **183**, 1760 (2012).
- [37] M.-J. Hwang and M.-S. Choi, *Phys. Rev. A* **82**, 025802 (2010).
- [38] M. Liu, Z.-J. Ying, J.-H. An, and H.-G. Luo, *New J. Phys.* **17**, 043001 (2015).
- [39] A. Le Boité, *Adv. Quantum Technol.* **3**, 1900140 (2020).
- [40] J. Liu, M. Liu, Z.-J. Ying, and H.-G. Luo, *Adv. Quantum Technol.* **4**, 2000139 (2021).
- [41] L. Cong, X.-M. Sun, M. Liu, Z.-J. Ying, and H.-G. Luo, *Phys. Rev. A* **95**, 063803 (2017).
- [42] L. Cong, X.-M. Sun, M. Liu, Z.-J. Ying, and H.-G. Luo, *Phys. Rev. A* **99**, 013815 (2019).
- [43] X.-M. Sun, L. Cong, H.-P. Eckerle, Z.-J. Ying, and H.-G. Luo, *Phys. Rev. A* **101**, 063832 (2020).
- [44] Z. Ying, *Adv. Quantum Technol.* **5**, 2100165 (2022).
- [45] E. K. Irish, J. Gea-Banacloche, I. Martin, and K. C. Schwab, *Phys. Rev. B* **72**, 195410 (2005).
- [46] Y. Chu, S. Zhang, B. Yu, and J. Cai, *Phys. Rev. Lett.* **126**, 010502 (2021).
- [47] Z. J. Ying, S. Felicetti, G. Liu, and D. Braak, *Entropy* **24**, 1015 (2022).
- [48] J. Casanova, G. Romero, I. Lizuain, J. J. García-Ripoll, and E. Solano, *Phys. Rev. Lett.* **105**, 263603 (2010).
- [49] H. Q. Lin, M. X. Liu, S. Chesi, and H. G. Luo, *J. Phys.: Conf. Ser.* **1163**, 012003 (2019).
- [50] C. Gerry, P. Knight, and P. L. Knight, *Introductory Quantum Optics* (Cambridge University, New York, 2005), p. 161.
- [51] M.-J. Hwang and M. B. Plenio, *Phys. Rev. Lett.* **117**, 123602 (2016).
- [52] A. Kenfack and K. Życzkowski, *J. Opt. B* **6**, 396 (2004).